



www.sciencedirect.com

Separation Purification Technology



Journal of Separation Science and Technology

SEPARATION AND PURIFICATION TECHNOLOGY

Volume 154 (2015)

Editor-in-Chief

B. Van der Bruggen (Heverlee, Belgium)

Editors

R. Aires-Barros (Lisboa, Portugal)
G. Chen (Kowloon, Hong Kong)
A. de Haan (Enschede, Netherlands)
B.V. Ramarao (Syracuse, USA)
Paul A. Webley (Victoria, Australia)

Editorial Board

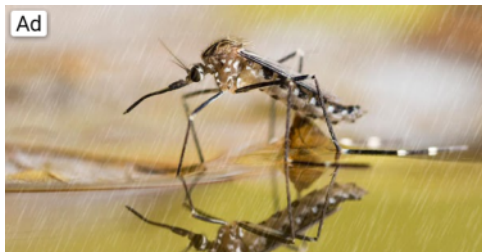
F.J. Alguacil (Madrid, Spain)
R. Bai (Singapore)
H. Bergmann (Köthen (Anhalt), Germany)
T. Cath (Golden, Colorado, USA)
X. Chen (Hangzhou, China)
L. Chu (Chengdu, China)
A. Denizli (Ankara, Turkey)
E. Drioli (Arcavacata di Rende (CS), Italy)
S. Farooq (Singapore)
X. Feng (Waterloo, Ontario, Canada)
T. Gu (Ohio, USA)
G. He (Dalian, China)
R.-S. Juang (Chungli, Taiwan)
S. Judd (Cranfield, Bedford, England, UK)
W.F. Leung (Hong Kong, China)
H. Liu (Beijing, China)

P. Luis (Louvain-la-Neuve, Belgium)
M.A. Rodrigo (Real, Spain)
A.E. Rodrigues (Porto, Portugal)
M. Sillanpaa (Lappeenranta, Finland)
D. Stamatialis (Enschede, Netherlands)
G. Stevens (Parkville, Victoria, Australia)
Y. Sun (Tianjin, China)
A. Szymczyk (Rennes, France)
D. Thomas (Nancy, France)
C. Tsouris (Oak Ridge, Tennessee, USA)
M. Ulbricht (Essen, Germany)
S. Vigneswaran (Broadway, New South Wales, Australia)
E. Vorobiev (Compiègne, France)
H. Yoshida (Tokyo, Japan)
M. Zhou (Tianjin, China)



ELSEVIER

Amsterdam • Boston • London • New York • Oxford • Paris •
Philadelphia • San Diego • St. Louis



Prevent Mosquitoes Breeding

Don't let mosquitoes find it easy to survive and breed within your property. Call us.

Rentokil Indonesia

OPEN

SCI Journal Impact Factor Database



ICETESTM Indonesia 2020

OPEN

Separation And Purification Technology

Basic Journal Info

Country



United Kingdom (<https://www.scijournal.org/country/united-kingdom>)

Journal ISSN: 13835866

Publisher: Elsevier Ltd. (<https://www.scijournal.org/publishers/elsevier-ltd>)

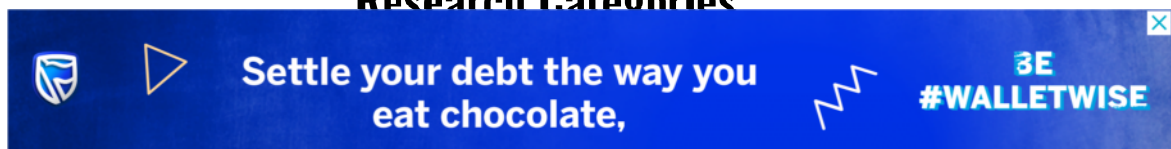
History: 1997-ongoing

Journal Homepage: Link (https://www.elsevier.com/wps/find/journaldescription.cws_home/600251/description#description)

Note:

You can find more information about getting published on this journal here: <https://www.elsevier.com/journals/separation-and-purification-technology/1383-5866/guide-for-authors>

Research Categories



Separation and Purification Technology

**2-year
Impact Factor**

6.195

**3-year
Impact Factor**

6.140

**4-year
Impact Factor**

5.829

Scope/Description:

Separation and Purification Technology is a publication dedicated to the dissemination of separation research results and findings. Its coverage extends to all aspects of separation and purification of homogeneous solutions and heterogeneous mixtures. Separation and Purification Technology welcomes, from investigators worldwide, contributions focused on the experimental studies and theoretical analyses of phenomena associated with and arising from separation and purification as well as process development and simulation, equipment design and fabrication and materials preparation and modification used in separation operations.



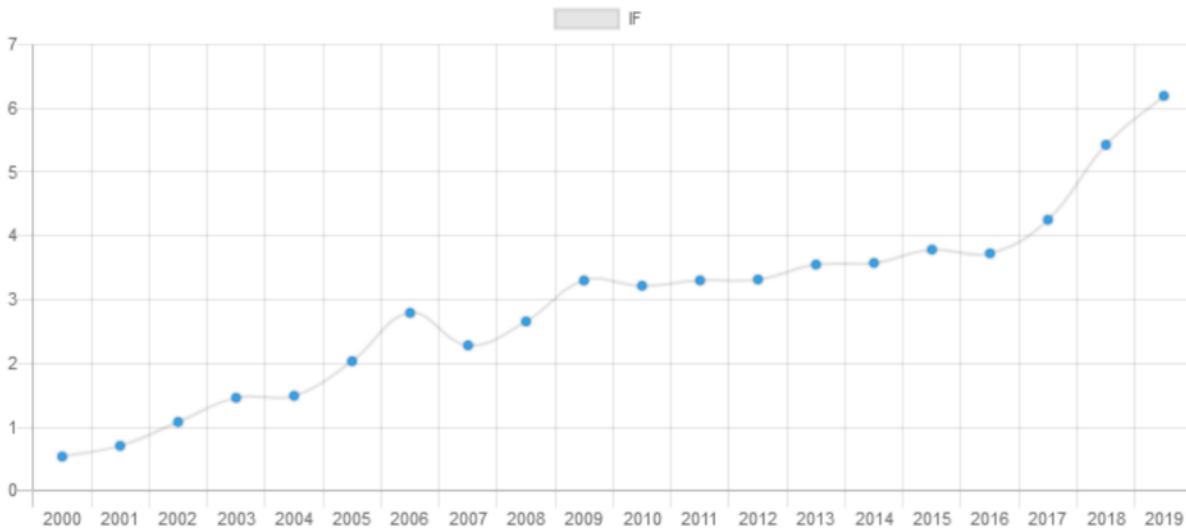
ICS Publications Store - Shipping Publications

Visit Site

Separation And Purification Technology

2-year Impact Factor Trend

JOURNAL IMPACT FACTOR DETAILS



Note: impact factor data for reference only

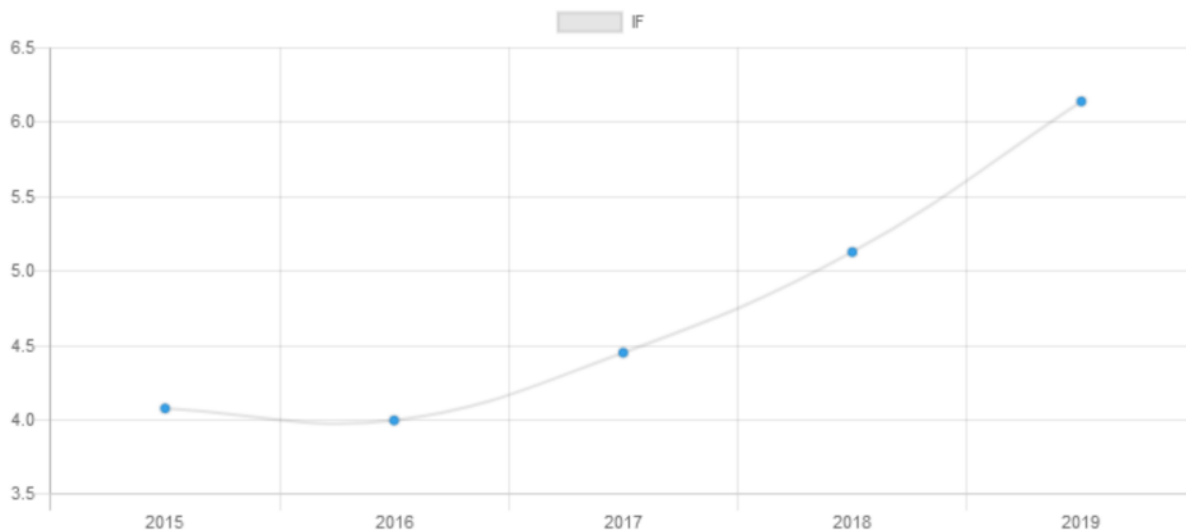


Publish your Research Paper

OPEN

3-year Impact Factor Trend

JOURNAL IMPACT FACTOR DETAILS



Note: impact factor data for reference only

Ad

open publish.eu

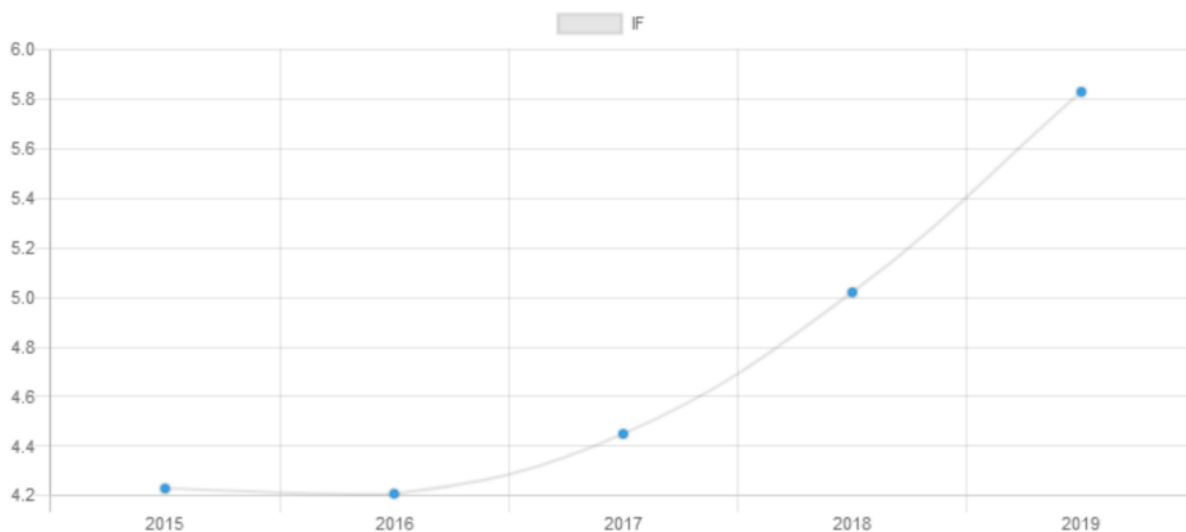
Indexed in SCOPUS and CPCI
OpenPublish.eu

Open >

Separation And Purification Technology

4-year Impact Factor Trend

JOURNAL IMPACT FACTOR DETAILS



Note: impact factor data for reference only

Impact Factor

The impact factor (IF) or journal impact factor (JIF) of an academic journal is a scientometric factor based on the yearly average number of citations on articles published by a particular journal in the last two years. In other words, the impact factor of 2020 is the average of the number of cited publications divided by the citable publications of a journal. A journal impact factor is frequently used as a proxy for the relative importance of a journal within its field. Normally, journals with higher impact factors are often deemed to have more influence than those with lower ones. However, the science community has also noted that review articles typically are more citable than research articles.

(Read More: What is a good impact factor?)

See what other people are reading

DISCOVER

Separation And Purification Technology

Impact Factor History

| | | |
|--|--------------------|-------|
| | 2019 Impact Factor | 6.195 |
| | 2018 Impact Factor | 5.427 |
| | 2017 Impact Factor | 4.253 |
| | 2016 Impact Factor | 3.726 |
| | 2015 Impact Factor | 3.785 |
| | 2014 Impact Factor | 3.576 |
| | 2013 Impact Factor | 3.551 |
| | 2012 Impact Factor | 3.317 |
| | 2011 Impact Factor | 3.303 |
| | 2010 Impact Factor | 3.218 |

| | |
|--------------------|-------|
| 2009 Impact Factor | 3.301 |
| 2008 Impact Factor | 2.659 |
| 2007 Impact Factor | 2.284 |
| 2006 Impact Factor | 2.794 |
| 2005 Impact Factor | 2.036 |
| 2004 Impact Factor | 1.493 |
| 2003 Impact Factor | 1.463 |
| 2002 Impact Factor | 1.083 |
| 2001 Impact Factor | 0.709 |
| 2000 Impact Factor | 0.541 |

Note: impact factor data for reference only

See what other people are reading

DISCOVER



How to Do a Competitive Analysis in 3 Steps

Other Journal Impact Indicator

Any journal impact factor or scientometric indicator alone will not give you the full picture of a science journal. That's why every year, scholars review current metrics to improve upon them and sometimes come up with new ones. There are also other factors to consider for example, H-Index, Self-Citation Ratio, SJR (SCImago Journal Rank Indicator) and SNIP (Source Normalized Impact per Paper). Researchers may also consider the practical aspect of a journal such as publication fees, acceptance rate, review speed.

[\(Read More\)](#)



How to Build an Impeccable Go-to-Market Strategy

Separation And Purification Technology

H-Index

The h-index is an author-level metric that attempts to measure both the productivity and citation impact of the publications of a scientist or scholar. The index is based on the set of the scientist's most cited papers and the number of citations that they have received in other publications

144

Separation And Purification Technology

SCImago Journal Rank (SJR)

SCImago Journal Rank (SJR indicator) is a measure of scientific influence of scholarly journals that accounts for both the number of citations received by a journal and the importance or prestige of the journals where such citations come from.

1.16



SCI JOURNAL

scijournal.org is a platform dedicated to making the search and use
of impact factors of science journals easier.

Copyright 2012-2020 scijournal.org



Scimago Journal & Country Rank

- Home
- Journal Rankings
- Country Rankings
- Viz Tools
- Help
- About Us

Separation and Purification Technology

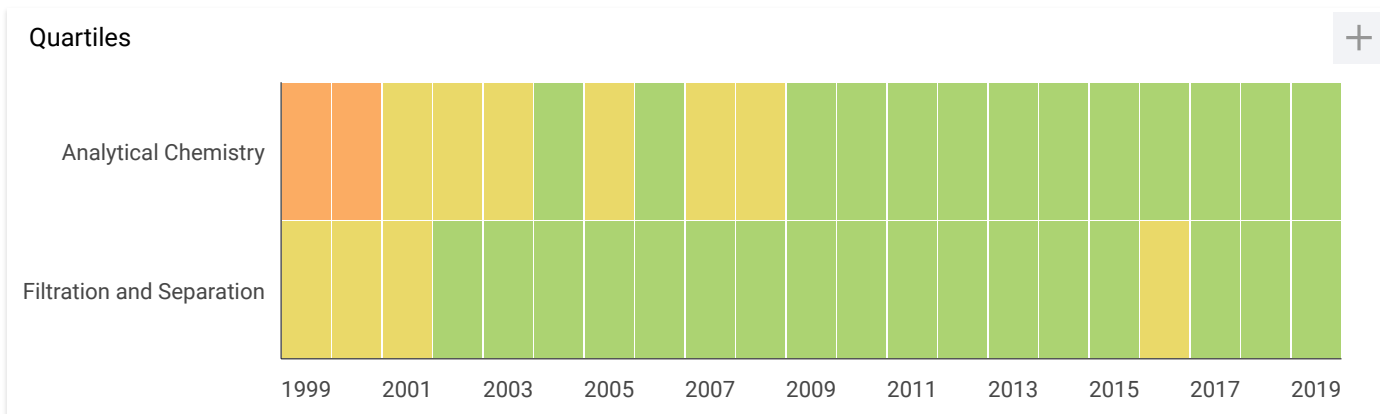
155

H Index

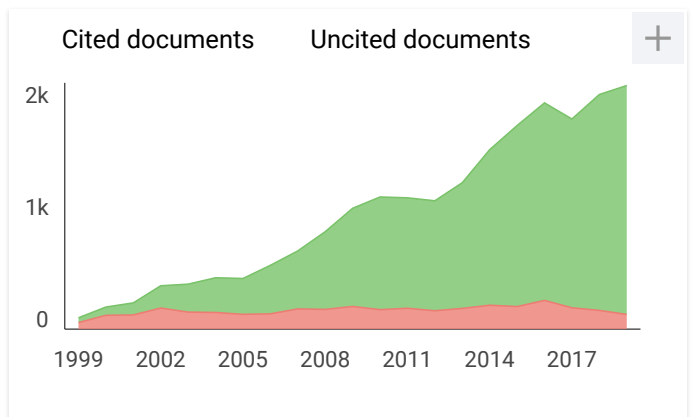
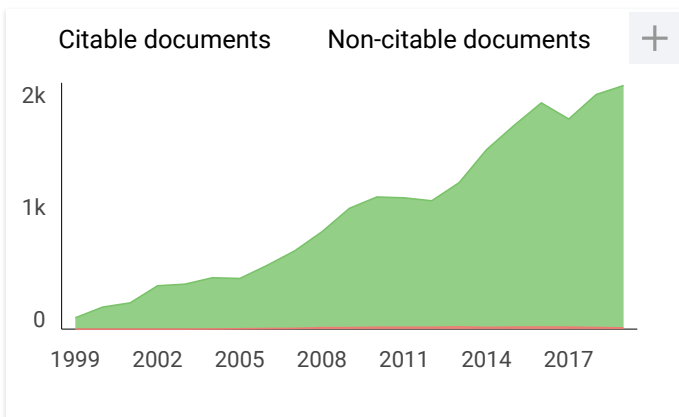
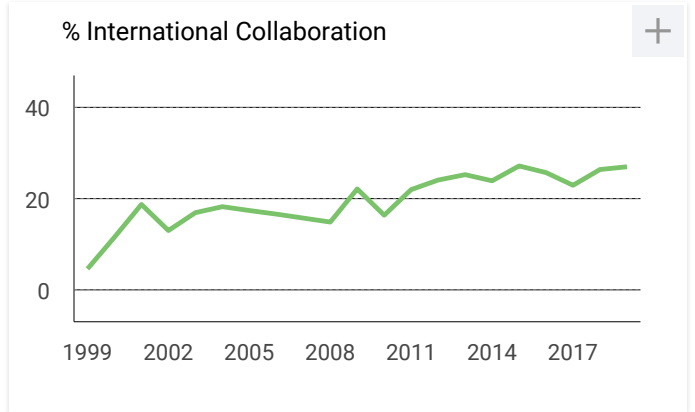
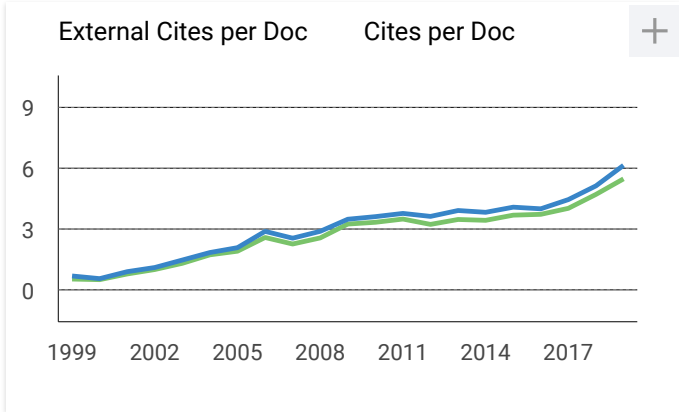
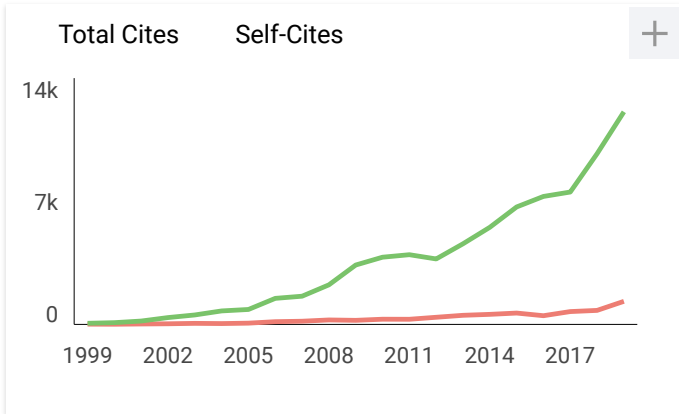
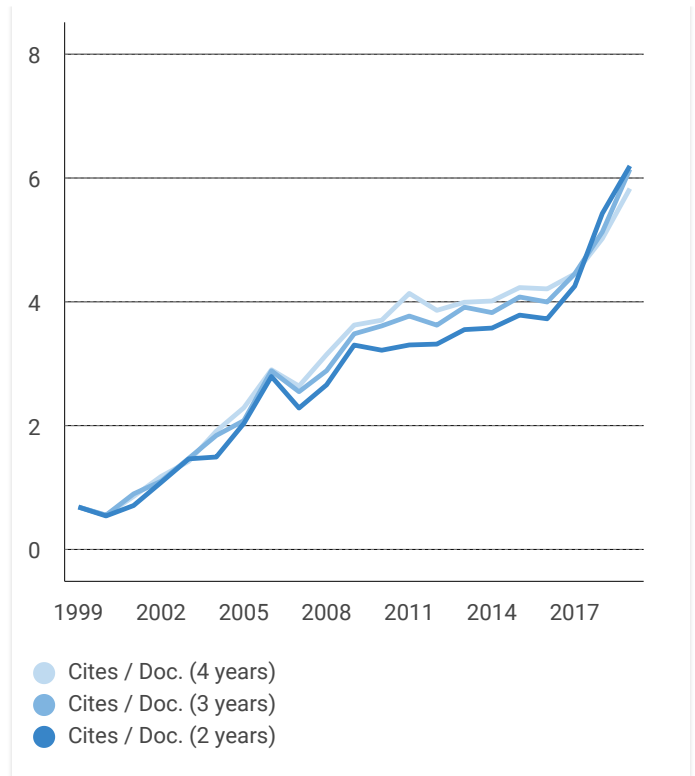
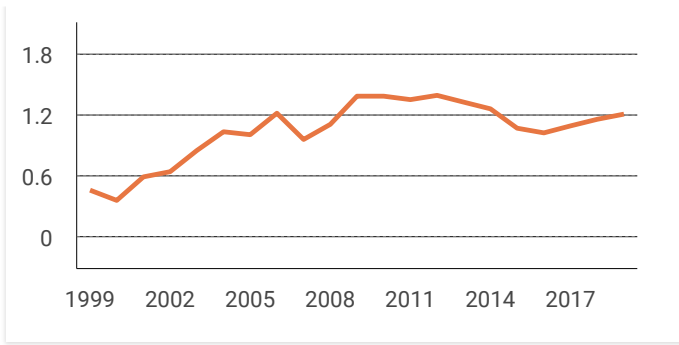
| | |
|----------------------------------|--|
| Country | Netherlands - SIR Ranking of Netherlands |
| Subject Area and Category | Chemical Engineering Filtration and Separation Chemistry Analytical Chemistry |
| Publisher | Elsevier |
| Publication type | Journals |
| ISSN | 13835866, 18733794 |
| Coverage | 1997-2020 |

Scope Separation and Purification Technology is a publication dedicated to the dissemination of separation research results and findings. Its coverage extends to all aspects of separation and purification of homogeneous solutions and heterogeneous mixtures. Separation and Purification Technology welcomes, from investigators worldwide, contributions focused on the experimental studies and theoretical analyses of phenomena associated with and arising from separation and purification as well as process development and simulation, equipment design and fabrication and materials preparation and modification used in separation operations.

- [Homepage](#)
- [How to publish in this journal](#)
- [Contact](#)
- [Join the conversation about this journal](#)



| | |
|--|---|
| SJR + | Citations per document + |
|--|---|



Separation and Purification Technology

Q1 Analytical Chemistry
best quartile

SJR 2019
1.21

powered by scimagojr.com

← Show this widget in your own website

Just copy the code below and paste within your html code:

```
<a href="https://www.scimagojr.com/journalsearch.php?q=14292&tip=sid&clean=0"
```

Metrics based on Scopus® data as of April 2020

M **Mohamed** 2 years ago

Hi,

I noticed that the journal impact factor has disappeared on the journal webpage although i have published an article early this year and the IF was close to 4. I am wondering whether there is accidently happened or what is going on?

Thanks

reply



Elena Corera 2 years ago

SCImago Team

Please, contact Separation and Purification Technology, you are contacting Scimago Journal and Country Rank.

Best,

SCImago Team

Leave a comment

Name

Email

(will not be published)

I'm not a robot
reCAPTCHA
Privacy - Terms

Submit

The users of Scimago Journal & Country Rank have the possibility to dialogue through comments linked to a specific journal. The purpose is to have a forum in which general doubts about the processes of publication in the journal, experiences and other issues derived from the publication of papers are resolved. For topics on particular articles, maintain the dialogue through the usual channels with your editor.

Developed by:



Powered by:



Follow us on @ScimagoJR

Scimago Lab, Copyright 2007-2020. Data Source: Scopus®

EST MODUS IN REBUS

Horatio (Satire 1,1,106)



Polyvinylidene fluoride membranes impregnated at optimised content of pristine and functionalised multi-walled carbon nanotubes for improved water permeation, solute rejection and mechanical properties



Jono Suhartono, Chedly Tizaoui*

Centre for Water Advanced Technologies and Environmental Research (CWATER), College of Engineering, Bay Campus, Swansea University, Swansea SA1 8EN, UK

ARTICLE INFO

Article history:

Received 11 June 2015

Received in revised form 9 September 2015

Accepted 11 September 2015

Available online 11 September 2015

Keywords:

Polyvinylidene fluoride membrane

Ultrafiltration

Multi-walled carbon nanotubes

Impregnation

ABSTRACT

Pristine (CNTs-P) and oxygen-plasma-functionalised (CNTs-O) multi-walled carbon nanotubes were incorporated in polyvinylidene fluoride (PVDF) membranes using the phase inversion technique. *N*-methyl 2-pyrrolidone solvent gave good dispersion and stability of the CNTs and hence was used for membrane fabrication. The membranes were characterised and their performances in water permeation and solutes (NOM, BrO₃⁻, Br⁻ and Cl⁻) rejection were evaluated at different CNT contents. SEM imaging of the membranes showed asymmetric finger-like porositic structure with small channelling tubes in the top layer that connect with larger channelling tubes in the deeper side. The finger-like pores were shallower in CNTs-O/PVDF membranes than the PVDF or CNTs-P/PVDF membranes. Due to oxygenated groups imparted by CNTs-O, CNTs-O/PVDF membranes were more wettable, presented higher electronegativity and hence better rejection of the anions. CNTs have increased membrane porosities and mean pore sizes and have lead to significantly enhanced water flux by up to 3.3 (CNTs-O) and 3.7 (CNTs-P) times that of pure PVDF membranes. They have also improved the rejections of NOM, bromate, bromide, and chloride at absolute values as high as 93.4%, 21.7%, 10.5%, and 9.2% respectively for CNTs-O/PVDF membrane. CNTs have also enhanced significantly the mechanical properties of the PVDF membranes and a CNT content of 0.2 mass% was optimal.

© 2015 Elsevier B.V. All rights reserved.

1. Introduction

Polyvinylidene fluoride (PVDF), $[-CH_2-CF_2-]_n$, is a highly hydrophobic semicrystalline, acid resistant and chemically inert polymer. It has recently gained considerable attention as one of the promising materials in polymeric membrane fabrication [1,2]. PVDF membranes have been widely used for fine separation processes, such as microfiltration, ultrafiltration, nanofiltration, membrane distillation, pervaporation and gas separation [2–4]. Techniques such as grafting and surface modification [5–7], addition of inorganic chemicals [8,9], and blending with other polymers [10,11] have been successfully used to modify the PVDF membrane porous structure and enhance its permeability, solute rejection, and fouling resistance. Impregnation of polymeric membranes with graphitic carbon materials has particularly attracted considerable attention in the last two decades [12]. Among the carbon materials, carbon nanotubes (CNTs) are very interesting materials to use for altering the properties of polymeric membranes. This is because

they possess high surface area, high aspect ratio, frictionless surfaces, simple functionalisation and good dispersion in common organic polymers. Research studies have found that CNTs increase membrane permeate flux and reduce roughness leading to enhanced membrane rejection and fouling resistance [13]. CNTs can also be functionalised to produce active functional groups (e.g. $-OH$, $=O$, $-COOH$, $-F$, $=N$, $-NH_2$) that enhance the separation of water solutes [14,15]. Besides, impregnation of CNTs increases the mechanical strength of the polymer and provides control of the pore dimensions at the nanometer scale [16]. Despite the many advantages offered by CNTs, studies on their use in PVDF nanocomposite membrane fabrication are scarce and it is only recently that few studies have started to emerge. Zhang et al. [17] have successfully used pristine and chemically oxidised MWCNTs to fabricate hybrid CNTs/PVDF membrane using the phase inversion method where *N,N*-dimethylacetamide (DMAc) was used as a solvent. They found that the addition of oxidised MWCNTs enhanced the hydrophilicity, permeability, antifouling and mechanical performances of the membrane. On the other hand, Madaeni et al. [15] embedded CNTs in PVDF by simply filtering a CNT solution through a commercial PVDF membrane. Xu et al. [18] have used the

* Corresponding author.

E-mail address: c.tizaoui@swansea.ac.uk (C. Tizaoui).

thermally induced phase separation to produce PVDF/O-MWCNT membranes with dense structure. They have also shown that the addition of O-MWCNTs improved the surface hydrophilicity (i.e. wettability) and the anti-fouling property of the membrane. In contrast, Ma et al. [19] have used a relatively high percentage of MWCNTs in PVDF (up to 2 mass%) and found that the water flux has increased by 11 times of that of pure PVDF membranes. They have also found that O-MWCNTs played a critical role in determining the morphologies and performances of the PVDF membranes impregnated with MWCNTs.

Although only very limited number of studies has been conducted so far on CNTs/PVDF membranes, the characteristics of the produced membranes are not well established and are difficult to predict since they are affected by many factors including the CNT type, its functionalisation, and its content in the polymer as well as the membrane fabrication conditions (e.g. solvent and non-solvent used, temperature, solution mixing conditions). This present study discusses the effects of the type and content of CNTs in modifying the properties of hybrid CNTs/PVDF membranes fabricated by the phase inversion technique. The study also evaluates the effects of CNT type and composition and membrane operating conditions on water permeation and solutes rejection.

2. Experimental

2.1. Materials

Analytical grade *N*-methyl-2-pyrrolidone (NMP), pristine multi-walled carbon nanotubes (CNTs-P), humic acid to represent natural organic matter (NOM), sodium bromate (NaBrO₃), and sodium bromide (NaBr) were purchased from Sigma Aldrich, UK whilst analytical grade of sodium chloride (NaCl) and *N,N*-dimethylformamide (DMF) were purchased from Fisher Scientific, UK. Polyvinylidene fluoride (PVDF) (Kynar 761 type) and plasma oxidised multiwalled carbon nanotubes (CNTs-O) were kindly supplied free of charge by Arkema, Ltd. and Haydale, Ltd. respectively. Both CNTs were used as received without further treatment. The pertinent physical properties of the CNTs from the manufacturers are shown in Table 1.

2.2. Fabrication of CNTs/PVDF membranes

Stock solutions of dispersed CNTs (see Supplementary Material) were made by adding an accurate mass of CNTs in 100 mL of solvent (i.e. NMP) to achieve concentrations of 0, 0.05, 0.1, 0.2, 0.3 and 0.4 mass% CNTs. The solutions were then ultrasonicated for 1 h before being used for membrane fabrication.

Kynar 761 PVDF powder was placed in an oven at 105 °C for 24 h to remove any moisture contained in the solid material. 4.12 g of dried PVDF powder was mixed with 20 mL of either pure NMP or NMP containing CNTs in a 60 mL glass beaker to obtain 20 mass% of polymer solution. This solution was then stirred at 250 rpm by a mechanical agitator (IKA-Werke GmbH & Co. KG, Germany) at 70 °C for 3 h to make sure that all PVDF was dissolved homogeneously. A water bath was used to control the operating temperature. After this mixing step, the solution was then cooled to 20 ± 1 °C in a desiccator to prevent exposure to water vapour.

Table 1

Properties of the carbon nanotubes from manufacturer.

| Property | CNTs-P | CNTs-O |
|-----------------------------------|--------|--------|
| Carbon content (%) | >95 | 96.08 |
| Outer diameter (nm) | 6–9 | ~13–16 |
| Length (μm) | 5 | ~1 |
| Aspect ratio (length/diameter) | ~667 | ~69 |
| Bulk density (g/cm ³) | 0.22 | ~0.19 |
| Oxygen content (%) | – | 3.5–4 |

Once the solution was bubble-free, it was then casted on a 30 × 35 cm smooth and clean glass plate. The membrane casting depth was set by a casting knife at 200 μm.

The casted membrane solution was then dipped in 25 L deionised water (DI) bath as soon as the casting process finished minimising solvent evaporation and exposure to air humidity. Solvent and non-solvent displacement and membrane coagulation were done at about 20 ± 1 °C. Although the coagulation took place very fast, the membrane was kept in the DI water bath for 2 h to ensure completion of the membrane formation process. Finally, the prepared membrane was stored in a DI water container at room temperature for testing.

2.3. Characterisation

The particle size distribution of CNTs in NMP were determined by High Performance Particle Sizer 3.3 (Malvern Instruments Ltd., UK) and their zeta-potential values were determined by a Zetasizer 2000 (Malvern Instruments Ltd., UK). Both of these measurements were presented as the average of 10 readings (results are in Supplementary Material). Viscosity of membrane solutions were determined by Ostwald BS/U tube viscometer size G (Rheotek, UK) at 30 °C. The membrane wettability was determined by contact angle measurements with a DAT 1100 (Fibro System ab, Sweden) using 4 μL of DI water as the wetting liquid and the contact angle was measured 12 s after the wetting liquid was dropped on the membrane. The measurement data were presented as average of five readings. Membrane zeta-potential values were determined by EKA Electrokinetic Analyser (Anton Paar GMBH, Austria) based on the streaming potential method. The analyses were made at pH 3.5–11 by a 10^{−3} M of KCl solution served as the electrolyte.

Polyethylene Glycol (PEG) of different molecular masses (3.35, 10, 20, and 35 kDa) and Polyethylene Oxide (PEO) of a 100 kDa molecular mass were used to determine the molecular weight cut off (MWCO) of the fabricated membranes by the solute transport method [20]. The concentration of PEG or PEO in the feed or permeate were determined by UV–VIS spectrophotometer (Agilent 8453, Agilent Technology, UK) at a wavelength of 192 nm [21,22]. Standard calibration curves ($R^2 > 0.995$) for each molecular size solute were prepared and used for the determination of solute concentrations.

The membrane volume porosity (ε) is defined as the ratio between the volume of the pores and the total volume of the porous membrane. The volume of the pores was determined from measurement of the volume of water that occupied the pores of a wetted membrane using a mass difference between a wet and dry membrane (Eq. (1)) [23,24].

$$\varepsilon = \frac{(m_{wet} - m_{dry})/\rho_l}{(m_{wet} - m_{dry})/\rho_l + m_{dry}/\rho_p} \times 100\% \quad (1)$$

where m_{wet} is the mass of wet membrane, m_{dry} is the mass of dry membrane, ρ_l is the density of water and ρ_p is the density of the polymer (in this study $\rho_p = 1.78 \text{ g/cm}^3$).

The mean pore radius, r_p , which represents the average pore size along the membrane thickness, was determined by the filtration velocity method according to the revised form Guerout–Elford–Ferry equation (Eq. (2)) [25,26].

$$r_p = \sqrt{\frac{(2.9 - 1.75\varepsilon) \times 8\eta l Q}{\varepsilon \Delta P}} \quad (2)$$

where l is the membrane thickness (m), η is the water viscosity ($8.9 \times 10^{-4} \text{ Pa s}$), ε is the membrane volume porosity determined as above, A is the membrane surface area (m²), Q is the flowrate of permeate (m³/s) and ΔP is the transmembrane operating pressure (Pa).

The molecular structure of the membrane was determined by a universal sampling attenuated total reflectance (ATR) combined with spectrum one Fourier Transform Infrared (FTIR) spectroscopy (PerkinElmer, UK) and the quantitative analysis of oxygen contained in the membrane was determined by an X-MAX silicon drift detector electron dispersive X-ray spectroscopy (Oxford Instrument, UK). The structure and surface imaging of the membranes were analysed using a Hitachi S4800 field emission scanning electron microscopy (SEM) (Hitachi, Japan). For the SEM analysis, the membrane samples were freeze-fractured and gold-coated before analysis. The freeze fracture was done by dipping the membrane in liquid nitrogen for several minutes then fractured as the membrane froze. The samples were then gold coated by sputter coater (Edwards, UK) at 20 mA for 15 s to create a gold coating thickness of approximately 3 nm.

The mechanical properties including tensile strength, elongation at the break point and Young modulus of dry membranes were investigated at room temperature with a Hounsfield Universal Testing Machine (Hounsfield UTM, UK now known as Tinius Olsen, Ltd., UK) (100 N max load cell) using a strain rate of 50 mm/min. The membrane sample sizes were length = 5 cm, width = 1 cm and thickness = 100 μm as determined by a micrometer. The mechanical results were averaged from four samples.

2.4. Membrane operation

Water permeation and solute rejection of the fabricated pristine PVDF and CNTs/PVDF membranes were evaluated using a cross-flow ultrafiltration membrane system. The membrane effective area was 9.6 cm^2 and the retentate water flowrate was set at 1 L/min whilst the transmembrane pressure (TMP) was set at 1.80, 2.80 or 4.85 bar. The mass of permeate was measured as function of time by a digital analytical balance connected to a computer for automatic data logging. The permeate flux, as determined from the slope of the line representing permeate mass versus time divided by the effective membrane area, was measured for about 15 min and it was started after the first 5 mL of permeate were collected. Membrane rejection of NOM (10 mg/L), bromate (200 $\mu\text{g/L}$), bromide (1 mg/L), and chloride (1000 mg/L) were also evaluated using the various membranes manufactured in this study. Although the fabricated membranes are expected to fall in the ultrafiltration pore size range and hence they may not be adequate for significant salt rejection, the use of salt in this study was to provide understanding whether the impregnation of CNTs in the membrane modifies salt rejection, possibly, based on charge repulsion and/or adsorption. The concentrations of NOM were measured by the UV-Vis spectrophotometer using a pre-determined calibration curve at a wavelength of 254 nm. The concentrations of the anions were determined using an ion chromatograph Dionex ICS-900 (Dionex Corporation, Sunnyvale, CA) equipped with IonPacTM AS14A (4 \times 250 mm) analytical column, IonpacTM AG14A (4 \times 50 mm) guard column and a DS5 suppressed conductivity detector with suppressor AMMSTM 300 4 mm. The eluent was 8 mM $\text{Na}_2\text{CO}_3/1.0$ mM NaHCO_3 . The IC was interfaced with a PC for data acquisition and analysis using the Chromeleon[®] software. Calibration curves were determined using standard solutions of the anions at different concentrations.

3. Results and discussion

3.1. Membrane characterisation

3.1.1. Contact angle

The wettability properties of membranes can be determined by measuring the contact angle between the membrane surface and

water as a wetting liquid. In general, high contact angles mean that the material is more difficult to wet. Fig. 1 compares the averaged contact angles at different contents of pristine and oxidised CNTs. It can be observed that higher content of CNTs-P added into the polymer matrix resulted in higher contact angles meaning that CNTs-P make the membranes less wettable. However, increasing the content of CNTs-O resulted in more wettable surfaces since the contact angle was reduced as the content of CNTs-O increased. The change in contact angle could be linked to the presence of CNTs on the surface of the membrane. Overall, when the CNT content changed from 0% to 0.4%, the contact angles have changed from 73.2° to 69.8° and 77.3° for CNTs-O/PVDF and CNTs-P/PVDF membranes respectively. This indicates that CNTs have modified the surface energy of the PVDF membranes. Given that CNTs are hydrophobic materials, the addition of their pristine version to the membrane made it less wettable than the pristine PVDF membrane. However, owing to the oxygen-rich functional groups present on the surface of CNTs-O, the wettability of the CNTs-O/PVDF membrane has fairly increased. It can be estimated from contact angle measurements that the oxidised functional groups on the surface of CNTs have increased the wettability of the membrane by up to 4.72%. Albeit virgin PVDF membranes are hydrophobic, impregnation of oxygen-functionalised CNTs in the membrane polymer casting matrix increases the wettability of the membrane thus providing better resistance to fouling [27].

3.1.2. Membrane zeta potential

Measurements of the membrane zeta potential illustrate that all three membranes show negative charges when used at neutral pH 7 (Fig. 2). The isoelectric points were almost similar for all membranes with values of 4.5 for pristine PVDF and 4.0 for both CNTs/PVDF membranes. However, as the pH increased above the isoelectric points, the CNTs-O/PVDF membrane became more negatively charged as compared to CNTs-P/PVDF and PVDF membranes. For example at pH 7, the zeta potential values are -22.43 , -16.87 and -12.77 mV for CNTs-O/PVDF, CNTs-P/PVDF and pristine PVDF membranes respectively. This shows that the addition of CNTs in the PVDF matrix, which as revealed before are characterised by negatively charged surfaces at pH 7, has naturally increased the negative charge of the membranes. Besides, oxidised functional groups (e.g. C–OH, C=O, C–OOH) imparted by CNTs-O reduce the zeta potential even further by providing more ionic or molecular interaction between CNTs and ions contained in water [28] thus resulting in increased accumulation of negative charges on the membrane surface.

3.1.3. Membrane porosity

The addition of carbon nanotubes into the PVDF polymer up to 0.4 mass% resulted in increased membrane porosities from that of

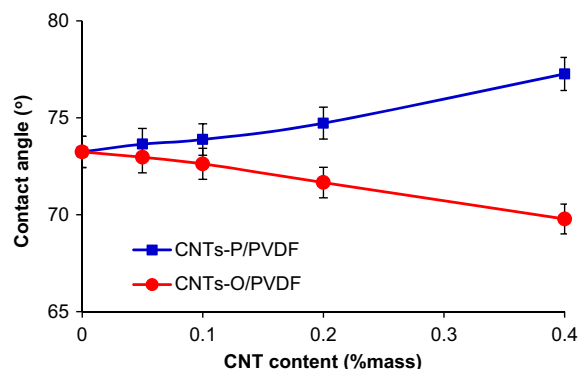


Fig. 1. Contact angle of CNTs-O/PVDF and CNTs-P/PVDF membranes.

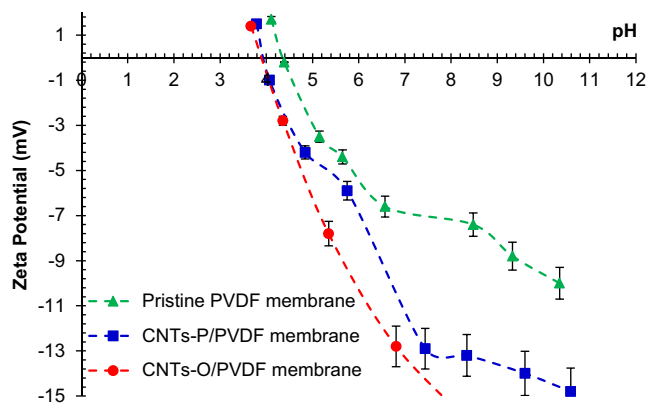


Fig. 2. Zeta potential of membranes (CNT at 0.3 mass%).

virgin PVDF membrane. Fig. 3 shows that the addition of 0.05 mass % of CNTs has increased membrane porosities by about 10% and 16% for CNTs-O and CNTs-P respectively. A further increase in the content of CNTs resulted in a maximum porosity at about 0.1 mass% for CNTs-P and at 0.2 mass% for CNTs-O membranes; porosity increased from 64% at 0% CNTs to 76% and 73% for CNTs-P and CNTs-O membranes at 0.1 mass% and 0.2 mass% respectively. The increase of porosity may due to the additional porosity imparted by the CNTs themselves, which are naturally hollow materials, as well as the formation of new macro-void porous structure resulting from the interaction of solid–liquid contacting body in the presence of suspended CNTs in the polymer matrix. Fig. 3 further shows that the additions of carbon nanotubes by more than 0.1 mass% for CNTs-P and by more than 0.2 mass% for CNTs-O lead to a decreased porosity. This reduction in porosity may be explained by agglomeration and entanglement of CNTs, at a relatively high concentration, causing reduction of macro-void porous formation. Besides, more CNTs increase the viscosity of the mixture CNTs/polymer (Table 2) resulting in delayed transfer rate between solvent and non-solvent during membrane formation [13]. The higher the viscosity of the CNTs/polymer matrix solution, the more reduction in the ability of water to penetrate the solution hence giving more time for the solvent in the solution to desolvate. Under this delayed demixing condition, more micro-void pores are formed and the top membrane layer becomes denser, thicker and with lower porosity [29,30,13].

Since hydrophilic materials tend to be easily wetted by water, the transfer of water during coagulation in CNTs-O/PVDF membrane is expected to be faster than in CNTs-P/PVDF membrane. As a result of higher water (i.e. non-solvent) transfer during membrane formation, higher porosity is hence expected in the CNTs-O/PVDF membrane matrix [23]. However, as shown in

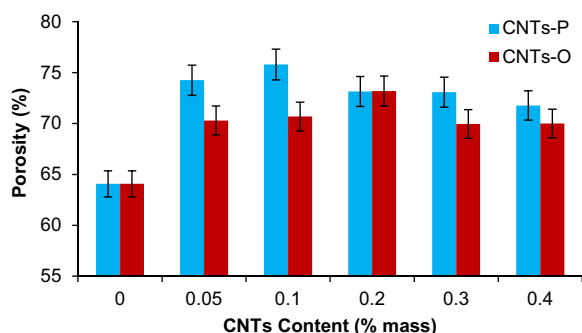


Fig. 3. Membrane porosities as function of CNTs content.

Table 2

Viscosity ratio between CNTs/PVDF solution and PVDF solution as function of CNT contents.

| CNTs content in PVDF solution (mass%) | Viscosity ratio | |
|---------------------------------------|-----------------|-------------|
| | CNTs-P/PVDF | CNTs-O/PVDF |
| 0 | 1 | 1 |
| 0.05 | 1.08 | 1.15 |
| 0.1 | 1.12 | 1.21 |
| 0.2 | 1.17 | 1.25 |
| 0.3 | 1.21 | 1.28 |
| 0.4 | 1.28 | 1.31 |

Fig. 3, CNTs-O/PVDF membranes have a slightly lower porosity than CNTs-P/PVDF membranes. This might be caused by the different dimensions and densities of the two CNTs used. As shown in Table 1 and as discussed in the Supplementary Material, CNTs-O used in this research has smaller aspect ratio than CNTs-P and also have smaller particle size than CNTs-P when dispersed in NMP. Smaller aspect ratio and particle size of CNTs-O provide more homogenous distribution in the solvent and makes CNTs-O less prone to entanglement between each other. In addition, the lighter density of CNTs-O as compared to CNTs-P also reduces the membrane porosity since for the same CNT mass used, CNTs-O will have more volume occupied and distributed in the polymer matrix. Therefore, CNTs-O, which are characterised by smaller dimensions, lighter density and higher viscosity suspension (Table 2) provide favourable conditions for the formation of micro-void pores hence reduced porosity as compared to CNTs-P [13].

3.1.4. Membrane mean pore size and MWCO

The mean pore size of the membranes and their MWCO at different CNT contents are shown in Table 3. According to this table, as the content of CNTs-O increased from 0% to 0.2%, the mean pore sizes have also increased from 10.56 to 15.41 nm respectively and a further addition of CNTs-O at contents higher than 0.2% decreased the mean pore size to 12.77 nm at 0.4%. Similar trend was also observed when CNTs-P were used with the mean pore sizes increasing from 10.56 nm at 0% to 15.91 nm at 0.2% followed by a decrease to 11.62 nm at 0.4% CNTs-P. This trend is in general agreement with that observed for the porosity above and also consistent with the water flux results that are discussed below which have also showed optima at 0.2% CNTs. Other studies have also observed similar trend when nanomaterials are incorporated in the polymer matrix [12]. The addition of a hydrophilic filler in the casting solution leads to an accelerated solvent and non-solvent exchange, hence encouraging formation of more porous polymeric structure [17]. However, a further increase in the filler content increases significantly the viscosity of the casting solution

Table 3

MWCO and mean pore size for membranes at various CNT types and contents.

| Membrane type | CNTs content (mass%) | MWCO (kDa) | Mean pore size (nm) |
|---------------|----------------------|------------|---------------------|
| Pure PVDF | 0 | 72.9 | 10.56 |
| CNTs-O/PVDF | 0.05 | 88.6 | 9.84 |
| | 0.1 | 92.8 | 12.06 |
| | 0.2 | 96.9 | 15.41 |
| | 0.3 | 78.5 | 13.52 |
| | 0.4 | 85.5 | 12.77 |
| CNTs-P/PVDF | 0.05 | 96.5 | 13.74 |
| | 0.1 | 92.9 | 14.42 |
| | 0.2 | 102 | 15.91 |
| | 0.3 | 92.9 | 12.41 |
| | 0.4 | 89.6 | 11.62 |

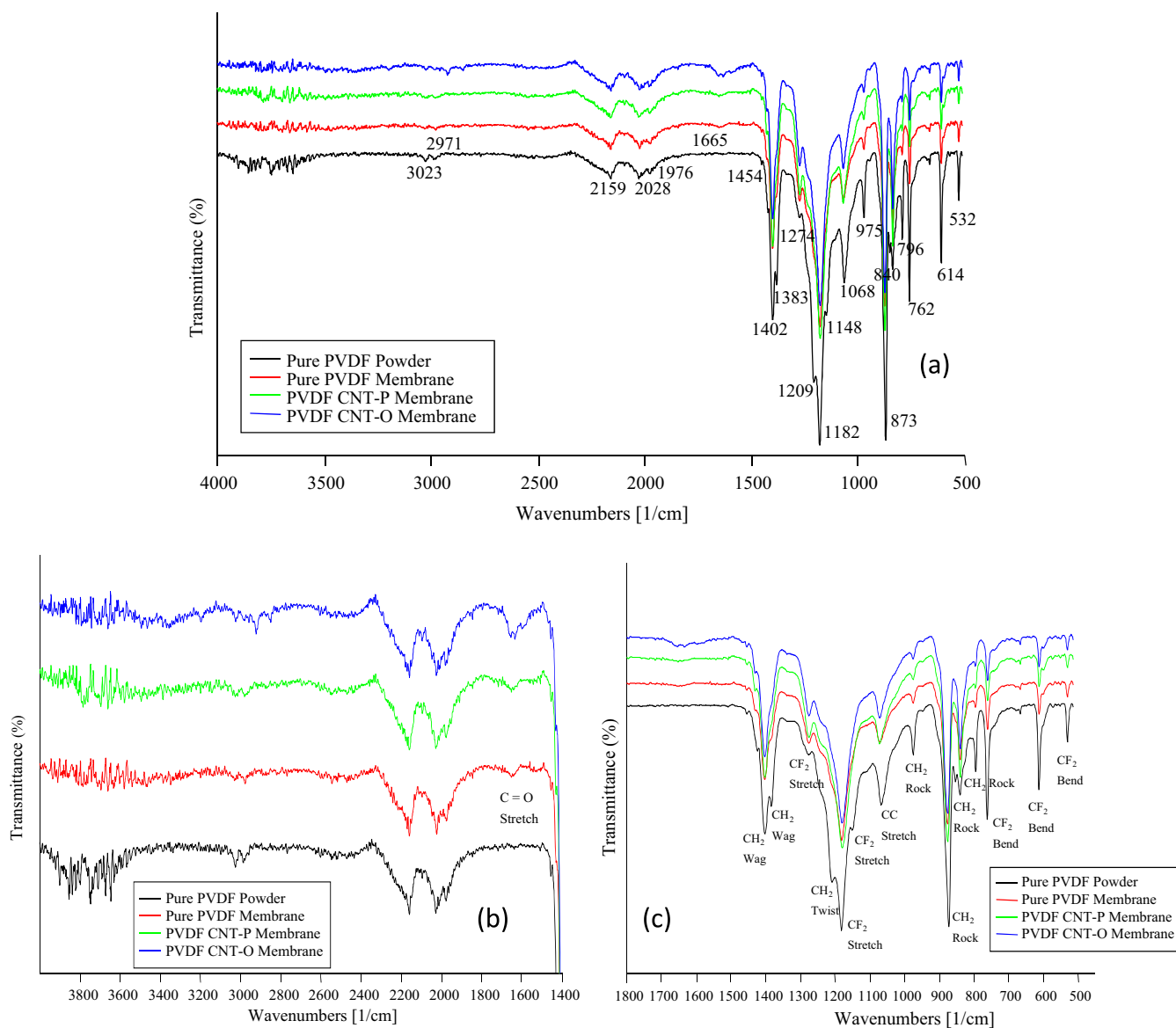


Fig. 4. FTIR-ATR spectra of fabricated membranes: (a) full band range; (b) 1400–4000 cm^{-1} band range; and (c) 500–1800 cm^{-1} band range (CNT content = 0.3%).

(Table 2) and thus a reduction in the exchange rate between solvent and non-solvent during membrane formation by the phase inversion technique resulting in reduced mean pore sizes.

The results in Table 3 also show that the MWCO followed similar trend as the mean pore size. It increased from 72.9 kDa to 96.9 kDa then decreased to 85.5 kDa as the percentages of CNTs-O increased from 0% to 0.2% then to 0.4% respectively. When CNTs-P were used, the MWCO also increased from 72.9 kDa to 102 kDa then declined to 89.6 kDa as the percentage of CNTs-P increased from 0% to 0.2% then to 0.4% respectively. The results in Table 3 supports that the PVDF-based membranes fabricated in this study fall in the category of ultrafiltration membranes. Comparing the effect of CNTs-P to CNTs-O on pore sizes, it appears that the incorporation of CNTs-P promoted a slightly higher pore sizes than CNTs-O particularly at low contents. This is in agreement with the trend of porosity observed earlier. However, it appears to be in disagreement with the expectation that the hydrophobic interaction between PVDF and CNTs-P to be strong which would lead to tighter pores. As shown by the ATR-FTIR results in Fig. 4, the conversion from a highly non-polar α -phase PVDF into a polar β -phase PVDF during the dissolution of PVDF into

the solvent seems to have weakened the bondings between CNTs-P and the polymer. As the CNTs-P/polymer bondings are weakened, they become conjugated by the solvent thus creating larger pores when replaced by the non-solvent during the immersion process.

3.1.5. FTIR-ATR

The chemical structure of a few-micrometer thick surface layer reflected by ATR-FTIR spectra of the membranes is shown in Fig. 4, where the wavenumbers applied were from 4000 to 500 cm^{-1} . The vibration peak bands reflected on the spectrum at 532, 614 and 763 cm^{-1} are accounted for CF_2 bending whilst spectrum bands at 796, 840, 873, and 975 cm^{-1} correspond to CH_2 rocking [31]. The groups of C–C symmetric stretching are characterised by the peak at 1068 cm^{-1} whilst stretching of the groups of CF_2 are at peaks 1148, 1182, and 1274 cm^{-1} [31,32]. The vibration band at 1209 cm^{-1} accounts for CH_2 twisting whilst the bands at 1383 and 1402 cm^{-1} account for CH_2 wagging [31]. Deformation of CH_2 groups occur at the peak 1454 cm^{-1} whilst the peaks at 2930 and 2967 cm^{-1} are assigned to the CH_2 symmetric and asymmetric stretching vibration modes [33,34].

The infrared absorption at 762, 840 and 1234 cm^{-1} might be selected as representative absorptions for the determination of the PVDF crystalline phase where higher value at 762 cm^{-1} represents the α -phase whilst higher peaks at 840 and 1234 cm^{-1} represent the γ -phase [35,36]. The presence of peaks at 840 cm^{-1} and 1274 cm^{-1} also indicates the formation of high electrical properties of β -phase forms [37,38]. An absorption band in the range 1440 cm^{-1} to 1000 cm^{-1} is important because it indicates the transformation from α -phase to β or γ -phases [39]. As shown in Fig. 4(a) and (c), the PVDF powder exhibits significantly higher peak at 762 cm^{-1} as compared to the fabricated membranes, which exhibit stronger peaks at 840 cm^{-1} and 1274 cm^{-1} instead, indicate that the PVDF powder is mostly α -phase crystalline and the fabricated membranes are mainly in the β -phase crystalline form.

New peak spectra in the fabricated membranes have occurred at about 1600–1700 cm^{-1} (Fig. 4(b)), which can be associated to the vibration of newly introduced functional carbonyl and carboxyl groups into the membranes [40,41]. The intensity of this peak is much stronger in the CNTs-O/PVDF membranes as compared to the pristine PVDF or CNTs-P/PVDF membranes. The presence of the oxygenated functional groups at higher intensity in the CNTs-O/PVDF membrane is obviously imparted by the oxygenated CNTs and the small peak shown in the other membranes may be formed during the membrane fabrication process. In fact, during the blending process of PVDF powder with the solvent NMP, which is done under relatively high temperature and inevitable exposure to air and moisture, NMP could degrade and produce amine products that contain carbonyl and carboxyl groups (e.g. methylamine, dimethylacetamide, amino carbonyl butanoic acid) [42,43]. The amine products in the solution dehydrofluorinate the PVDF and lead to amines addition to the PVDF chain accompanied by their conversion to carbonyl and carboxylic groups in the presence of oxygen in solution [44] as observed in Fig. 4(b). The formation of brownish colour in the solution during heating as observed in this study gives further evidence of the development of these reactions [44].

3.1.6. Energy Dispersive X-ray Spectroscopy (EDX)

For more detailed information about the oxygen content on the membrane and to ascertain the presence of oxygenated functional groups on the fabricated membranes, oxygen content was analysed by EDX (Fig. 5). Oxygen molecules were detected in all membranes including PVDF membranes without addition of CNTs and this is consistent with FTIR-ATR analysis results. Pristine PVDF and CNTs-P/PVDF (0.4 mass% CNTs-P) membranes were found to contain almost the same oxygen content of about 0.12%. However, the highest oxygen content was found in CNTs-O/PVDF membranes. For example at 0.4% CNTs-O, the membrane oxygen content was 0.137%, accounting for an increase of 13% from the oxygen content of pristine PVDF membrane (Fig. 5). Considering the oxygen content of CNTs-O being 4 mass% (Table 1), theoretically the addition of 0.4 mass% of CNTs-O leads to a membrane oxygen content of 0.136% which agrees well with the experimental value reported above.

3.1.7. Scanning electron microscopy (SEM)

Images showing the colour gradation of CNTs/PVDF membranes were taken by digital photography as presented in Fig. 6(a). As the CNT content increased, darker membrane colours were imaged. The porous membrane structure with CNTs impregnated on the membrane is shown by SEM micrographs (Fig. 6(b)–(f)). Fig. 6(d–f) shows that the manufactured membranes exhibit an asymmetric with finger-like structure and cavities of different sizes and shapes beneath the skin layer. This structure agrees with those of PVDF membranes presented in the literature [40]. The total thickness of the membrane was about $100 \pm 10 \mu\text{m}$ when measured by

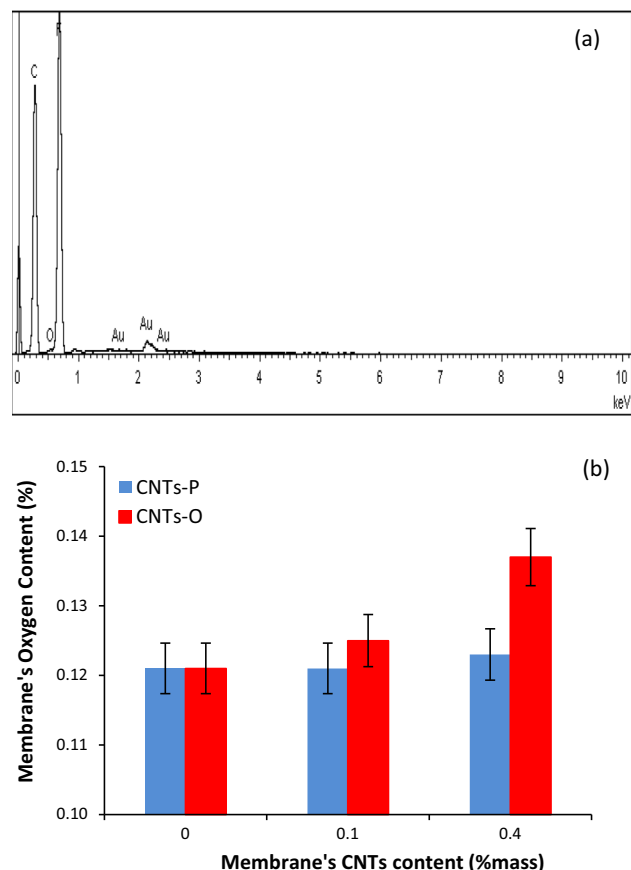


Fig. 5. (a) EDX spectra of 0.4 mass% CNTs-O and (b) oxygen content of fabricated 0.4% CNTs-O/PVDF membranes.

SEM, which is close to the expected thickness. Using SEM images, it was possible to estimate an average pore size of the active skin layer of the membrane in the order of 30 nm. This was also checked using the AFM technique (data not shown here). Zhang and Vecitis [45] have also reported pore sizes of a CNT/PVDF membrane, measured by SEM, in the same order of magnitude (28 nm). The finger-like pores on the membrane support have diameters of about 2–15 μm whilst the cavity pores have diameters in the range 200–500 nm. The occurrence of denser top layer can be explained by faster desolvation of solvent into the non-solvent medium and this occurs before the non-solvent penetrates the casted membrane [46,47]. The growth of the dense top layer will be halted when sufficient non-solvent medium have diffused into the sublayer solution to create the pores. The porous surface forms when the non-solvent inflow is higher than the solvent outflow [23]. Fig. 6(d–f) also shows that small channelling tubes in the top layer connect with larger channelling tubes in the lower side and this will result in high permeation and excellent solute rejection. Fig. 6(e and f) also shows that the addition of CNTs resulted in reduction of the finger-like structure of the membranes, possibly due to delayed solvent/non-solvent replacement during the coagulation process as a result of increased viscosity imparted by CNTs (Table 2). This result is in agreement with that obtained by Zhao et al. [24].

3.1.8. Mechanical properties

The membranes at different CNT contents were tested for stress–strain characteristics and the results for the Young modulus (i.e. elastic tensile modulus), stress at the break point, and the elongation at the break point were determined and plotted in Fig. 7(a–c). As shown in Fig. 7(a), Young's modulus raises as

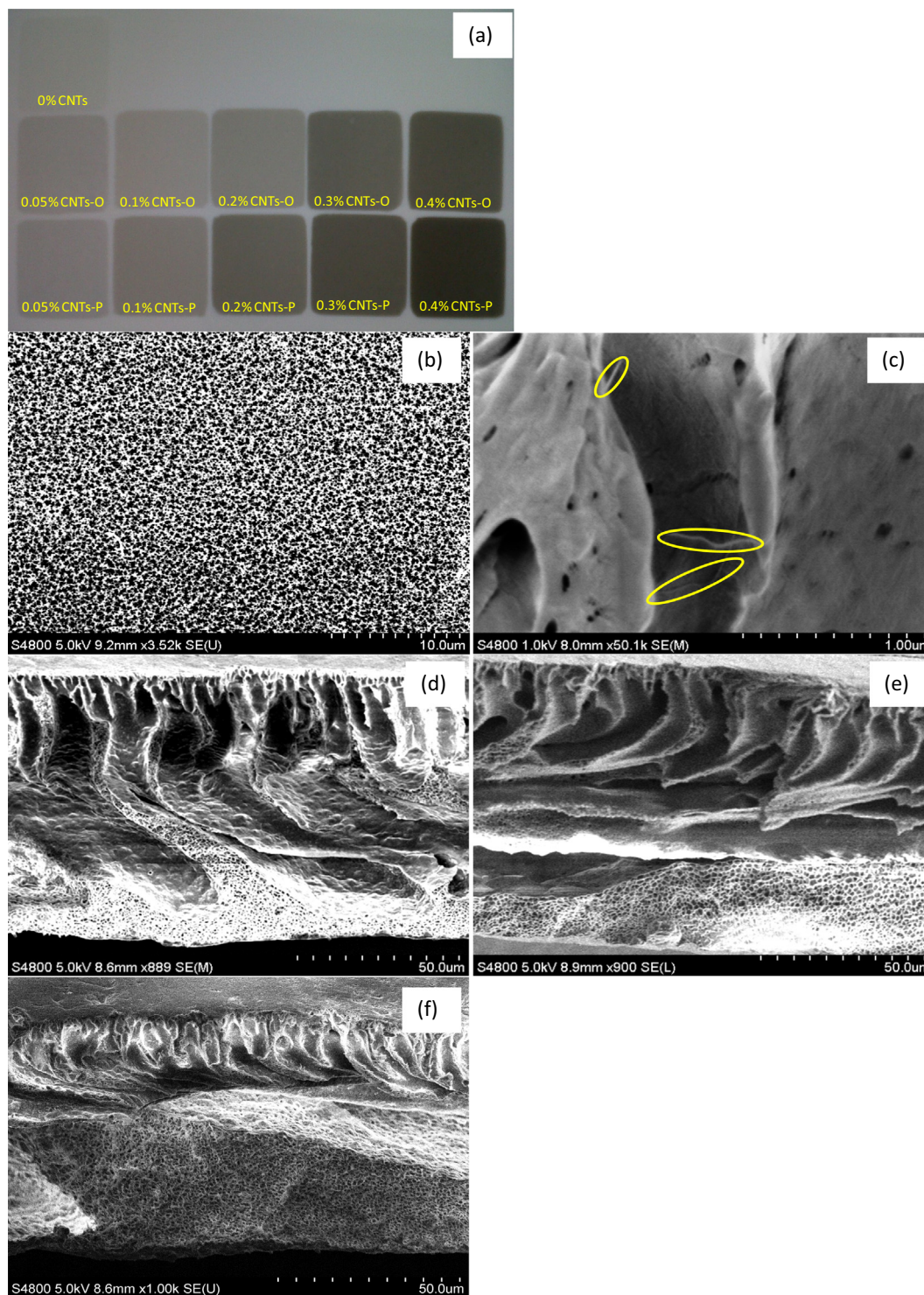


Fig. 6. (a) Digital photograph of top membrane sides; (b) SEM image of 0.4 mass% CNTs/PVDF membrane top layer side; (c) SEM image of impregnated 0.4 mass% CNTs-O in membrane (CNTs are shown by yellow ovals); SEM cross section images of the fabricated membranes: (d) pure PVDF; (e) CNTs-P/PVDF; and (f) CNTs-O/PVDF.

the CNT content increases up to 0.2% from 67.3 MPa for pure PVDF membrane to 105.4 MPa and 92.1 MPa for CNTs-P and CNTs-O respectively. This indicates that CNTs have reinforced the composite membrane by increasing its resistance to elastic deformation. CNTs-O appear to have lower effect than CNTs-P possibly as a result of lower interaction between the PVDF and CNTs-O due to weak interface compatibility between hydrophilic CNTs-O and hydrophobic PVDF matrix. As the percentage of CNTs is further

increased above 0.2%, Young's modulus decreases sharply (62.9 MPa at 0.4% CNTs-O). Ma et al. [19] have also found that 0.2% O-MWCNT gave the highest tensile strength. The stress at break point has also followed a similar trend (Fig. 7(b)) whereby it increased from 2.4 MPa for pure PVDF membrane to 3.1 MPa and 2.9 MPa for 0.2% CNTs-P and CNTs-O respectively then declined as the CNTs content increased further. The effect of CNTs on the elongation at break point up to a content of 0.3% is less

pronounced since it remained almost constant at $41.7 \pm 4\%$ and $44.2 \pm 5\%$ for CNTs-P and CNTs-O respectively (Fig. 7(c)). A further increase of CNTs content to 0.4%, however, has sharply reduced the elongation at break point to 16.9% and 18.6% for CNTs-P and CNTs-O respectively. This indicates that the addition of higher CNTs content in the casting solution results in brittle membranes. The mechanical properties of the CNTs/PVDF membranes strongly depend on the interaction between the polymer and the CNTs. The incorporation of the CNTs in the polymer matrix could increase the crystallinity of the composite membranes and thus enhance their mechanical properties. However, higher CNT contents might promote aggregation of the CNTs thus resulting in weaker interaction between the polymer matrix and the CNTs leading to reduction of the Young's modulus and elongation at the break point. The results obtained in this study indicate that the mechanical properties of the PVDF membranes were significantly enhanced via the addition of CNTs at an optimum content of 0.2 mass% with CNTs-P being slightly better than CNTs-O.

3.2. Membrane performance

3.2.1. Water permeation

Fig. 8(a–c) shows the changes of the pure water flux as function of transmembrane pressure and CNT content. Fig. 8(a and b) shows that the addition of CNTs-O or CNTs-P into the polymer matrix resulted in higher membrane water flux than without CNTs. The water flux continued to increase up to 0.2 mass% CNTs then decreased as further additions of CNTs were made. This trend is consistent with that observed for the membrane pore sizes that also showed a convex profile with increasing CNT content. A CNT content of 0.2 mass% can then be taken as optimum for water flux. At 0.2 mass% CNTs, the flux has increased from that of pure PVDF membrane at TMPs of 1.8, 2.8, 4.9 bar by 3.3, 3.0, and 2.0 times for CNTs-O and by 3.7, 3.2, and 2.1 times for CNTs-P respectively. This indicates that CNTs have improved the water flux of the membranes and the content 0.2 mass% of both CNTs appears as an optimum. The presence of CNTs in the PVDF membrane leads to the formation of more porous areas and larger pore sizes (Fig. 3 and Table 3), which results in reduced hydraulic resistance and hence enhanced permeate flux [30,13,48].

Comparing pristine to oxidised CNTs, Fig. 8(a and b) shows that for lower CNT content less than 0.2 mass%, the water flux of CNTs-P/PVDF membrane tends to be higher than that of CNTs-O/PVDF membrane (by about 30% on average). This can be directly attributed to the larger pores of CNTs-P/PVDF membranes at lower CNTs content (Table 3). However, this trend reverses slightly as the content of CNT increased beyond 0.2 mass%. At higher CNT additions, the slightly higher mean pore size of CNTs-O/PVDF membrane (Table 3) may have provided lower membrane resistance and hence higher permeation than CNTs-P/PVDF membranes. Besides, the increased wettability of CNTs-O/PVDF membrane as CNTs-O content increased (Fig. 1) has potentially elevated the wettability of the membrane also resulting in higher water permeation. Membrane wettability (i.e. lower contact angle) is known to enhance the water permeability by attracting water molecules inside the membrane pores facilitating their passage through the membrane.

Fig. 8(c) shows that higher transmembrane pressure (TMP) increased water flux for all membranes. Naturally, higher TMP increases the driving force of water permeation resulting in faster water penetration into the membrane pores and producing higher flux. Depending on the content of CNTs used, as TMP increased from 1.8 to 4.85 bar, the water flux values have also increased by for example 3.2 times for both CNTs at a content of 0.2 mass%. The values of the permeability (i.e. Flux/TMP) were calculated and averaged over the various TMPs used. Permeability values at 0.2% CNTs of

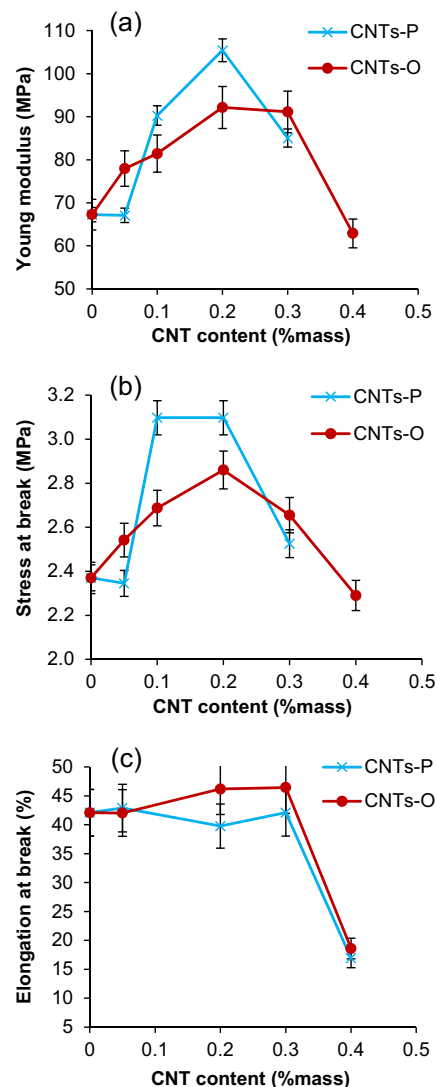


Fig. 7. Mechanical properties of the CNTs/PVDF membranes as function of CNT content (a) Young's modulus; (b) stress at break point; and (c) elongation at break point.

$38.7 \pm 2.0 \text{ L/m}^2 \text{ h bar}$ and $41.3 \pm 2.1 \text{ L/m}^2 \text{ h bar}$ were obtained for CNTs-O/PVDF and CNTs-P/PVDF membranes respectively.

3.2.2. Solute rejection

Fig. 9 shows the rejection percentages for NOM and the anionic solutes bromate, bromide, and chloride at pH 7. Fig. 9(a) reveals that as expected, the PVDF membrane (i.e. 0% mass CNTs) exhibited small rejections of the three anionic solutes of 9.1%, 5.1% and 3.8% for bromate, bromide and chloride respectively. However, impregnation of CNTs in the PVDF membranes have increased the rejection of the anions; for example at 0.4 mass% CNTs, rejections of bromate, bromide and chloride have increased to 21.7% (CNTs-O/PVDF) and 19.6% (CNTs-P/PVDF), to 10.5% (CNTs-O/PVDF) and 8.8% (CNTs-P/PVDF), and to 9.2% (CNTs-O/PVDF) and 7.8% (CNTs-P/PVDF) respectively. Daraei et al. [48] have also showed that rejection of anions was enhanced by the addition of CNTs to their polyethersulfone membrane. Fig. 9 also shows that the membrane rejection for bromate, bromide and chloride follows the order: PVDF < CNTs-P/PVDF < CNTs-O/PVDF. Meanwhile, the rejections of the three anions follow the order: $\text{Cl}^- < \text{Br}^- < \text{BrO}_3^-$. Charge repulsion between the anions and the negatively charged surface of the

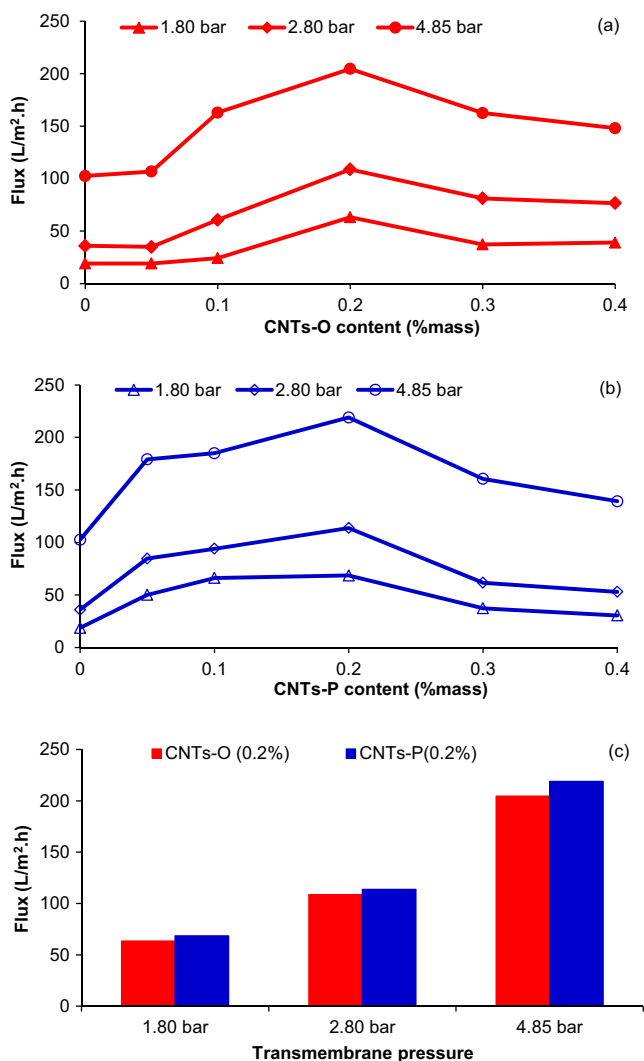


Fig. 8. Membrane water flux as function of CNTs content and transmembrane pressure, (a) CNTs-O/PVDF membrane; (b) CNTs-P/PVDF membrane; and (c) membrane water flux as function of operating transmembrane pressure at 0.2 mass% CNTs content.

membranes (at pH 7 membrane ZPs are -13 mV (PVDF), -17 mV (CNTs-P/PVDF) and -23 mV (CNTs-O/PVDF) (Fig. 2)) could be largely responsible for the rejection of the anions observed in this study. It should be noted that the order of anions rejection by the three membranes follows the same order as the surface charge. Previous studies have also shown that due to the membrane surface charge, ultrafiltration or nanofiltration membranes can reject ions, even though the pore size of the membrane is much larger than the size of the ions [49–52].

The rejection of NOM was significantly higher than the anions at a percentage of 90.0% for PVDF membrane and modestly increased for CNTs impregnated PVDF membranes to about 93.4% (Fig. 9(b)). The rejection of NOM by CNTs-O/PVDF membrane was slightly higher than that by CNTs-P/PVDF membrane. The rejection of NOM by the PVDF membranes with or without CNTs may be attributed to a combined effect of charge repulsion (at the experiment's pH 7 both NOM molecules and the surface of the membranes are negatively charged) and by steric hindrance due to the relatively large NOM molecules and the aggregates they form on the surface of the membrane. Despite that CNTs have only increased NOM rejection by a small percentage, 3.4% at best for CNTs-O/PVDF, their addition to the PVDF membranes has

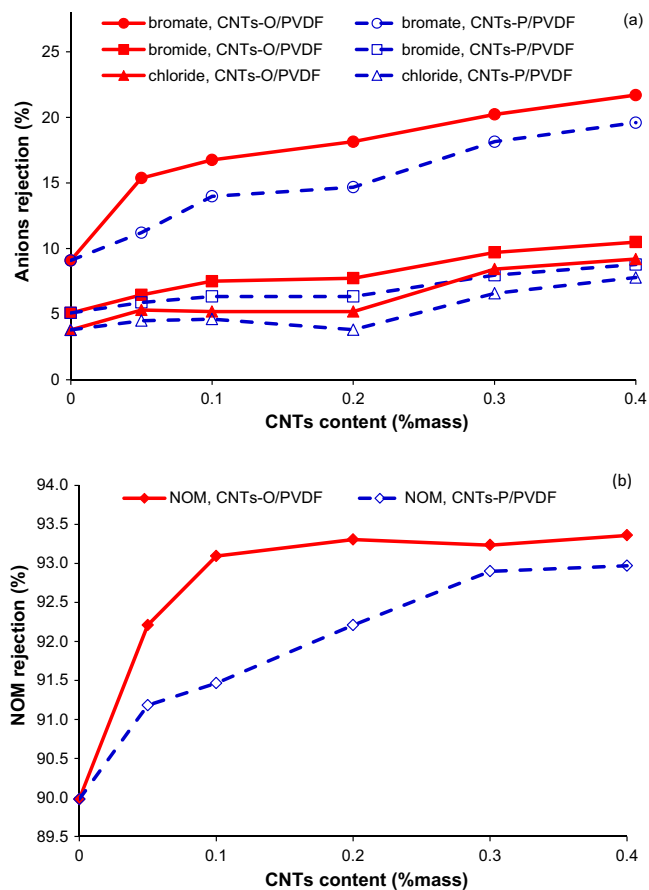


Fig. 9. Membrane solute rejection performance as function of CNTs loading: (a) bromate, bromide and chloride rejection; (b) NOM rejection operated at pH 7, TMP 3.85 bar and retentate flowrate 1 L/min.

significantly increased the water flux in the presence of NOM as compared to pristine PVDF membranes. In addition and given that CNTs have significantly enhanced anions rejection and the mechanical properties of the membranes, it is therefore evident that CNTs/PVDF (particularly CNTs-O) membranes have a promising potential application in water purification at enhanced water permeation and solutes rejection.

4. Conclusions

Fabrication of new membranes is required for a range of separation applications such as water treatment. This study has successfully fabricated composite PVDF membranes by the phase inversion technique and optimised the content of two types of multiwalled carbon nanotubes CNTs-O and CNTs-P as membrane fillers. The study showed that NMP was an excellent dispersing solvent for both CNTs, though the presence of oxidised functional groups on the plasma oxidised CNTs gave a better affinity of the CNTs-O towards NMP. Moreover, the oxidised functional groups have not only increased the dispersion of CNTs-O in NMP but have also increased the electronegativity of the fabricated membranes (see Supplementary Material).

Detailed membrane structure shows that all membranes have finger-like structures with the shallowest depth obtained in CNTs-O/PVDF membranes whilst the deepest pores were obtained in pure PVDF membranes. The ATR-FTIR analysis revealed that the fabricated PVDF membranes have β -phase crystalline structure. CNTs-O/PVDF membranes tend to be more hydrophilic whilst CNTs-P/PVDF tend to be more hydrophobic. Low CNT content in

the membranes up to about 0.2 mass% have increased the membrane porosity and mean pore sizes, which resulted in increased water permeation. However, further addition of CNTs decreased membrane permeation possibly due to blockage of the pores as a result of CNT agglomeration. The mechanical properties of the membranes have also been enhanced by the addition of the CNTs with a CNT content of 0.2 mass% being optimal. The fabricated membranes exhibited enhanced rejection of anionic solutes, particularly bromate, as a result of CNTs impregnation in the PVDF membrane though NOM rejection was modestly increased by less than 3.4% in the presence of CNTs. CNTs-O appear to provide slightly lower water permeability than CNTs-P but higher solute rejection. Given the significant enhancement in water permeation and the enhanced rejection of solutes in addition to improved mechanical properties, CNTs-O/PVDF membranes have a great potential to develop in a robust UF membrane technique for water purification.

Acknowledgements

Jono Suhartono would like to thank the Directorate General of Higher Education, Indonesia for their financial support of his PhD studies through grant number 397/E4.4/2011. Acknowledgement also goes to Haydale Ltd. for providing CNTs-O and Arkema Ltd. for providing PVDF powder. Many thanks to Dr. Paul M. Williams, Dr. Alex M. Lord, Dr. Peter Douglas and Mr. Ian Matthews from Swansea University for their help with the characterisation of the membranes.

Appendix A. Supplementary material

Supplementary data associated with this article can be found, in the online version, at <http://dx.doi.org/10.1016/j.seppur.2015.09.009>.

References

- [1] F. Liu, N.A. Hashim, Y. Liu, M.R.M. Abed, K. Li, Progress in the production and modification of PVDF membranes, *J. Membr. Sci.* 375 (1–2) (2011) 1–27.
- [2] G.-D. Kang, Y.-M. Cao, Application and modification of poly(vinylidene fluoride) (PVDF) membranes – a review, *J. Membr. Sci.* 463 (2014) 145–165.
- [3] M.G. Buonomenna, L.C. Lopez, P. Favia, R. d'Agostino, A. Gordanò, E. Drioli, New PVDF membranes: the effect of plasma surface modification on retention in nanofiltration of aqueous solution containing organic compounds, *Water Res.* 41 (19) (2007) 4309–4316.
- [4] P. Sukitpaneevit, T.-S. Chung, L.Y. Jiang, Modified pore-flow model for pervaporation mass transport in PVDF hollow fiber membranes for ethanol-water separation, *J. Membr. Sci.* 362 (1–2) (2010) 393–406.
- [5] A. Bottino, G. Capannelli, O. Monticelli, P. Piaggio, Poly(vinylidene fluoride) with improved functionalization for membrane production, *J. Membr. Sci.* 166 (1) (2000) 23–29.
- [6] N.A. Hashim, F. Liu, K. Li, A simplified method for preparation of hydrophilic PVDF membranes from an amphiphilic graft copolymer, *J. Membr. Sci.* 345 (1–2) (2009) 134–141.
- [7] Z. Zheng, Z. Gu, R. Huo, Z. Luo, Fabrication of self-cleaning poly(vinylidene fluoride) membrane with micro/nanoscaled two-tier roughness, *J. Appl. Polym. Sci.* 122 (2) (2011) 1268–1274.
- [8] A. Bottino, G. Capannelli, A. Comite, Preparation and characterization of novel porous PVDF-ZrO₂ composite membranes, *Desalination* 146 (1–3) (2002) 35–40.
- [9] E. Fontananova, J.C. Jansen, A. Cristiano, E. Curcio, E. Drioli, Effect of additives in the casting solution on the formation of PVDF membranes, *Desalination* 192 (1–3) (2006) 190–197.
- [10] L. Yan, J. Wang, Development of a new polymer membrane – PVB/PVDF blended membrane, *Desalination* 281 (2011) 455–461.
- [11] N. Pezeshk, R.M. Narbaitz, More fouling resistant modified PVDF ultrafiltration membranes for water treatment, *Desalination* 287 (2012) 247–254.
- [12] J. Yin, B. Deng, Polymer-matrix nanocomposite membranes for water treatment, *J. Membr. Sci.* 479 (2015) 256–275.
- [13] V. Vatanpour, S.S. Madaeni, R. Moradian, S. Zinadini, B. Astinchap, Fabrication and characterization of novel antifouling nanofiltration membrane prepared from oxidized multiwalled carbon nanotube/polyethersulfone nanocomposite, *J. Membr. Sci.* 375 (1–2) (2011) 284–294.
- [14] G.P. Rao, C. Lu, F. Su, Sorption of divalent metal ions from aqueous solution by carbon nanotubes: a review, *Sep. Purif. Technol.* 58 (1) (2007) 224–231.
- [15] S.S. Madaeni, S. Zinadini, V. Vatanpour, Convective flow adsorption of nickel ions in PVDF membrane embedded with multi-walled carbon nanotubes and PAA coating, *Sep. Purif. Technol.* 80 (1) (2011) 155–162.
- [16] S. Reich, C. Thomsen, J. Maultzsch, Carbon Nanotubes: Basic Concepts and Physical Properties, Wiley-VCH, Weinheim, 2004.
- [17] J.G. Zhang, Z.W. Xu, W. Mai, C.Y. Min, B.M. Zhou, M.J. Shan, Y.L. Li, C.Y. Yang, Z. Wang, X.M. Qian, Improved hydrophilicity, permeability, antifouling and mechanical performance of PVDF composite ultrafiltration membranes tailored by oxidized low-dimensional carbon nanomaterials, *J. Mater. Chem. A* 1 (9) (2013) 3101–3111.
- [18] H.-P. Xu, W.-Z. Lang, X. Yan, X. Zhang, Y.-J. Guo, Preparation and characterizations of poly(vinylidene fluoride)/oxidized multi-wall carbon nanotube membranes with bi-continuous structure by thermally induced phase separation method, *J. Membr. Sci.* 467 (2014) 142–152.
- [19] J.L. Ma, Y.F. Zhao, Z.W. Xu, C.Y. Min, B.M. Zhou, Y.L. Li, B.D. Li, J.R. Niu, Role of oxygen-containing groups on MWCNTs in enhanced separation and permeability performance for PVDF hybrid ultrafiltration membranes, *Desalination* 320 (2013) 1–9.
- [20] S. Singh, K.C. Khulbe, T. Matsuura, P. Ramamurthy, Membrane characterization by solute transport and atomic force microscopy, *J. Membr. Sci.* 142 (1) (1998) 111–127.
- [21] L. Gajdos, L. Pietrelli, A. Ciccarello, J. Derco, Elimination of polyethylene glycol from aqueous solution using activated carbon, *Pol. J. Environ. Stud.* 16 (3) (2007) 385–388.
- [22] Z. JianBin, Z. PengYan, M. Kai, H. Fang, C. GuoHua, W. XiongHui, Hydrogen bonding interactions between ethylene glycol and water: density, excess molar volume, and spectral study, *Sci. China. Ser. B – Chem.* 51 (5) (2008) 420–426.
- [23] M.B. Thürmer, P. Poletto, M. Marcolin, J. Duarte, M. Zeni, Effect of non-solvents used in the coagulation bath on morphology of PVDF membranes, *Mater. Res.* 15 (6) (2012) 884–890.
- [24] Y. Zhao, Z. Xu, M. Shan, C. Min, B. Zhou, Y. Li, B. Li, L. Liu, X. Qian, Effect of graphite oxide and multi-walled carbon nanotubes on the microstructure and performance of PVDF membranes, *Sep. Purif. Technol.* 103 (2013) 78–83.
- [25] E. Yuliwati, A.F. Ismail, T. Matsuura, M.A. Kassim, M.S. Abdullah, Characterization of surface-modified porous PVDF hollow fibers for refinery wastewater treatment using microscopic observation, *Desalination* 283 (2011) 206–213.
- [26] V. Vatanpour, S.S. Madaeni, R. Moradian, S. Zinadini, B. Astinchap, Novel antifouling nanofiltration polyethersulfone membrane fabricated from embedding TiO₂ coated multiwalled carbon nanotubes, *Sep. Purif. Technol.* 90 (2012) 69–82.
- [27] D. Rana, T. Matsuura, Surface modifications for antifouling membranes, *Chem. Rev.* 110 (4) (2010) 2448–2471.
- [28] Y. Liu, L. Gao, J. Sun, Y. Wang, Functionalization of carbon nanotubes for nanoparticle attachment, *J. Ceram. Process. Res.* 11 (1) (2010) 120–122.
- [29] P. vandeWitte, P.J. Dijkstra, J.W.A. vandenBerg, J. Feijen, Phase separation processes in polymer solutions in relation to membrane formation, *J. Membr. Sci.* 117 (1–2) (1996) 1–31.
- [30] H. Wu, B. Tang, P. Wu, Novel ultrafiltration membranes prepared from a multi-walled carbon nanotubes/polymer composite, *J. Membr. Sci.* 362 (1–2) (2010) 374–383.
- [31] N. Shukla, A. Shukla, A.K. Thakur, R. Choudhary, Low temperature ferroelectric behaviour of PVDF based composites, *Indian J. Eng. Mater. Sci.* 15 (2) (2008) 126.
- [32] P. Nallasamy, S. Mohan, Vibrational spectroscopic characterization of form II poly(vinylidene fluoride), *Indian J. Pure Appl. Phys.* 43 (11) (2005) 821–827.
- [33] J. Mihály, S. Sterkel, H.M. Ortner, L. Kocsis, L. Hajba, É. Furdyga, J. Minka, FTIR and FT-Raman spectroscopic study on polymer based high pressure digestion vessels, *Croat. Chem. Acta* 79 (3) (2006) 497–501.
- [34] J.-Q. Meng, C.-L. Chen, L.-P. Huang, Q.-Y. Du, Y.-F. Zhang, Surface modification of PVDF membrane via AGET ATRP directly from the membrane surface, *Appl. Surf. Sci.* 257 (14) (2011) 6282–6290.
- [35] J.-W. Park, I. Kim, K. Aimi, S. Ando, C.-S. Ha, Solid-state ¹⁹F MAS NMR analysis of the γ -phase of poly(vinylidene fluoride), *Polym. Preprints* 45 (1) (2004) 951.
- [36] Y.J. Park, Y.S. Kang, C.M. Park, Micropatterning of semicrystalline poly(vinylidene fluoride) (PVDF) solutions, *Eur. Polym. J.* 41 (5) (2005) 1002–1012.
- [37] G. Mago, D.M. Kalyon, F.T. Fisher, Membranes of poly(vinylidene fluoride) and PVDF nanocomposites with carbon nanotubes via immersion precipitation, *J. Nanomater.* (2008).
- [38] S.C. Tjong, Y.-W. Mai, Physical Properties and Applications of Polymer Nanocomposites, Woodhead Publishing Limited, Cambridge, 2010.
- [39] B. Ahmed, S.K. Raghuvanshia, Siddhartha, N.P. Sharma, J.B.M. Krishna, M.A. Wahab, 1.25mev Gamma irradiated induced physical and chemical changes in poly(vinylidene fluoride) (PVDF) polymer, *Prog. Nanotechnol. Nanomater.* 2 (2) (2013) 42–46.
- [40] A. Bottino, G. Capannelli, A. Comite, Novel porous membranes from chemically modified poly(vinylidene fluoride), *J. Membr. Sci.* 273 (1–2) (2006) 20–24.
- [41] M. Zhang, Q.T. Nguyen, Z. Ping, Hydrophilic modification of poly(vinylidene fluoride) microporous membrane, *J. Membr. Sci.* 327 (1–2) (2009) 78–86.
- [42] C. Berruoco, P. Alvarez, S. Venditti, T.J. Morgan, A.A. Herod, M. Millan, R. Kandiyoiti, Sample contamination with NMP-oxidation products and byproduct-free NMP removal from sample solutions, *Energy Fuel* 23 (2009) 3008–3015.

- [43] D.W. Reynolds, M. Galvani, S.R. Hicks, B.J. Joshi, S.A. Kennedy-Gabb, M.H. Kleinman, P.Z. Parmar, The use of N-methylpyrrolidone as a cosolvent and oxidant in pharmaceutical stress testing, *J. Pharm. Sci.* 101 (2) (2012) 761–776.
- [44] A. Taguet, B. Ameduri, B. Boutevin, Crosslinking of vinylidene fluoride-containing fluoropolymers, *Adv. Polym. Sci.* 184 (2005) 127–211.
- [45] Q. Zhang, C.D. Vecitis, Conductive CNT-PVDF membrane for capacitive organic fouling reduction, *J. Membr. Sci.* 459 (2014) 143–156.
- [46] T.-H. Young, L.-P. Cheng, D.-J. Lin, L. Fane, W.-Y. Chuang, Mechanisms of PVDF membrane formation by immersion-precipitation in soft (1-octanol) and harsh (water) nonsolvents, *Polymer* 40 (19) (1999) 5315–5323.
- [47] W.Y. Chuang, T.H. Young, W.Y. Chiu, C.Y. Lin, The effect of polymeric additives on the structure and permeability of poly(vinyl alcohol) asymmetric membranes, *Polymer* 41 (15) (2000) 5633–5641.
- [48] P. Daraei, S.S. Madaeni, N. Ghaemi, H. Ahmadi Monfared, M.A. Khadivi, Fabrication of PES nanofiltration membrane by simultaneous use of multi-walled carbon nanotube and surface graft polymerization method: comparison of MWCNT and PAA modified MWCNT, *Sep. Purif. Technol.* 104 (2013) 32–44.
- [49] C. Labbez, P. Fievet, A. Szymczyk, A. Vidonne, A. Foissy, J. Pagetti, Analysis of the salt retention of a titania membrane using the “DSPM” model: effect of pH, salt concentration and nature, *J. Membr. Sci.* 208 (1–2) (2002) 315–329.
- [50] Y. Yoon, G. Amy, J. Cho, N. Her, J. Pellegrino, Transport of perchlorate (ClO_4^-) through NF and UF membranes, *Desalination* 147 (1–3) (2002) 11–17.
- [51] A.V.R. Reddy, D.J. Mohan, A. Bhattacharya, V.J. Shah, P.K. Ghosh, Surface modification of ultrafiltration membranes by preadsorption of a negatively charged polymer: I. Permeation of water soluble polymers and inorganic salt solutions and fouling resistance properties, *J. Membr. Sci.* 214 (2) (2003) 211–221.
- [52] M. Moslemi, S.H. Davies, S.J. Masten, Rejection of bromide and bromate ions by a ceramic membrane, *Environ. Eng. Sci.* 29 (12) (2012) 1092–1096.